Key Points:
- Annual fast ice cycle in the southeastern Laptev Sea is characterized
- The main factors controlling annual fast ice cycle are revealed
- The trends in timing of the annual cycle are estimated

Correspondence to:
V. Selyuzhenok,
valeria.selyuzhenok@awi.de

Seasonal and interannual variability of fast ice extent in the southeastern Laptev Sea between 1999 and 2013

V. Selyuzhenok[1], T. Krumpen[1], A. Mahoney[2], M. Janout[1], and R. Gerdes[1,3]

[1]Alfred-Wegener-Institut Helmholtz-Zentrum für Polar- und Meeresforschung, Bremerhaven, Germany, [2]Geophysical Institute, University of Alaska, Fairbanks, Alaska, USA, [3]Department of Physics and Earth Sciences, Jacobs University Bremen, Bremen, Germany

Abstract Along with changes in sea ice extent, thickness, and drift speed, Arctic sea ice regime is characterized by a decrease of fast ice season and reduction of fast ice extent. The most extensive fast ice cover in the Arctic develops in the southeastern Laptev Sea. Using weekly operational sea ice charts produced by Arctic and Antarctic Research Institute (AARI, Russia) from 1999 to 2013, we identified five main key events that characterize the annual evolution of fast ice in the southeastern Laptev Sea. Linking the occurrence of the key events with the atmospheric forcing, bathymetry, freezeup, and melt onset, we examined the processes driving annual fast ice cycle. The analysis revealed that fast ice in the region is sensitive to thermodynamic processes throughout a season, while the wind has a strong influence only on the first stages of fast ice development. The maximal fast ice extent is closely linked to the bathymetry and local topography and is primarily defined by the location of shoals, where fast ice is likely grounded. The annual fast ice cycle shows significant changes over the period of investigation, with tendencies toward later fast ice formation and earlier breakup. These tendencies result in an overall decrease of the fast ice season by 2.8 d/yr, which is significantly higher than previously reported trends.

1. Introduction

Numerous studies report that Arctic sea ice cover has experienced significant changes during the last three decades. Total Arctic sea ice extent shows a negative trend in all months since 1979, with a larger magnitude for the recent decade [*Comiso and Hall*, 2014; *Meier et al.*, 2014]. Along with the reduction of total extent, there are indications of sea ice thinning [*Rothrock et al.*, 1999; *Kwok et al.*, 2009; *Laxon et al.*, 2013] and increased sea ice drift speed [*Spreen et al.*, 2011] and deformation rate [*Herman and Glowacki*, 2012]. Long-term changes were also found in the fast ice regime. Investigating Kara Sea fast ice, *Divine et al.* [2003] found a reduction in fast ice area in March–May, 1990–2000 relative to 1950–1960. *Mahoney et al.* [2014] report on a decrease of fast ice extent and a trend toward later formation and earlier disappearance of fast ice in the Chukchi Sea during the last four decades. In addition, there are indications of fast ice thickness loss in the Siberian Arctic [*Polyakov et al.*, 2003, 2012]. These regional changes are reflected in Arctic-wide reduction in fast ice area and shortening of the fast ice season in the 1990s reported by *Yu et al.* [2014].

Although fast ice only comprises a small fraction of overall Arctic sea ice extent, it is of particular importance for the coastal systems for a number of reasons. The fast ice edge defines the location of polynyas and thereby controls local ocean processes governed by sea ice formation and brine rejection, as well as atmospheric mesoscale motion [*Maqueda et al.*, 2004]. Fast ice damps tidal motion and influence mixing processes by blocking the momentum flux from the atmosphere to the ocean [*Proshutinsky et al.*, 2007]. In central and east Siberia, bottom-fast ice helps to maintain submarine permafrost and protects the coast from erosion [*Rachold et al.*, 2000]. The presence of bottom-fast ice controls the spring freshwater outflow in the vicinity of river deltas [*Are and Reimnitz*, 2000]. In the Laptev Sea, fast ice plays a crucial role in the freshwater cycle of the ocean by storing a great amount of riverine freshwater in winter and releasing it in summer [*Bareiss and Gorgen*, 2005; *Eicken et al.*, 2005]. Fast ice also affects human activities. In the western Arctic, it serves as a platform for traditional hunting and fishing. The distribution of fast ice has significant implications for polar marine navigation and offshore exploration, particularly for the seas situated along the North-East passage [*Johannessen et al.*, 2005; *Hughes et al.*, 2011].

Fast ice forms seasonally in the majority of the Arctic marginal seas. The winter extent of fast ice varies strongly on a regional scale from tens of kilometers along Alaska's coast to hundreds of kilometers in the southeastern Laptev and East Siberian Seas. The regional differences in fast ice extent are often associated with local topography and bathymetry. On average, the fast ice edge is located within the 10–25 m depth range [*Zubov*, 1945; *Divine et al.*, 2004; *Mahoney et al.*, 2007a, b]. However, the factors governing interannual and seasonal variability of fast ice extent differ from region to region. According to *Dmitrenko et al.* [1999], the interannual variations in the location of fast ice edge in the Kara, Laptev, and East Siberian Seas are controlled by river runoff. In contrast, *Divine et al.* [2004, 2005] found that the typical maximum extent of fast ice in the Kara Sea is sensitive to the dynamic atmospheric forcing and the variability of fast ice extent can be explained by variations in surface winds and air temperature. In contrast to the Kara Sea, the typical maximum extent of fast ice along the northern Alaskan coast appears to be controlled largely by local bathymetry, although there is evidence of diminished fast ice extent in the Chukchi Sea since the 1970s [*Mahoney et al.*, 2014]. In the Laptev Sea, fast ice processes are closely linked with the Lena River runoff. First, Laptev Sea fast ice is primarily composed of the river water [*Eicken et al.*, 2005]. Second, there are indications that the position of fast ice edge in winter is predefined by the intensity of Lena River summer runoff [*Dmitrenko et al.*, 1999]. Third, spring fast ice breakup in the region is triggered when nearshore fast ice is flooded by river water [*Bareiss et al.*, 1999]. Although the southeastern Laptev Sea is characterized by the widest fast ice extent in the Arctic, no study has investigated the linkage between fast ice climatology and atmospheric forcing and bathymetry.

The first aim of this study is to examine seasonal evolution of fast ice extent in the southeastern Laptev Sea and link it to the onset of freezeup and melt, air temperature, wind, and bathymetry by analyzing 14 annual fast ice cycles between 1999 and 2013. As fast ice extent and duration of fast ice season has decreased during the last decades, our second aim is to examine the interannual variability and timing of fast ice season in the region.

2. Data and Methods

2.1. AARI Charts

The information on fast ice extent used in this study is taken from operational sea ice charts provided by the Arctic and Antarctic Research Institute (AARI), Russia. AARI produces the charts since 1933 to support marine navigation and to assist other commercial and scientific purposes. The charts show total sea ice concentration, partial concentration of different stages of sea ice development and fast ice. Sea ice conditions are mapped manually based on air reconnaissance flights, ship reports, observations from polar meteorological stations, drift buoys, and satellite imagery. A detailed description of data sources and chart production are provided in *Mahoney et al.* [2008]. Due to limited observational data, temporal and spatial coverage of charts are inconsistent from 1933 to 1998. Since 1999, the frequency of coverage is higher because charts are primarily based on satellite remote sensing data. Detailed regional charts for the Eurasian Arctic shelf seas are available on a weekly basis in a vector Sea Ice Grid format (SIGRID-3). Fast ice is classified based on the criteria of immobility as well as other visual attributes such as absence of leads in the sea ice cover. The information analyzed by an expert is compiled for a period of 2–5 days prior to the issue date while the previous chart is used as a reference. Therefore, fast ice is defined as sea ice cover which remains stationary along the coast during a period of 2–7 days.

In this study, 524 charts covering the period from October 1999 to December 2013 were used [*World Meteorological Organisation*, 2013]. For practical reasons, we converted the vector format to a grid (EASE-Grid 2.0) with 1.25 km cell size for the region of interest (Figure 1). Hereafter, the gridded data are referred to as AARI charts. Although the temporal and spatial data coverage is highest for the period after 1998, there are no data available between January and July 2002. There are a number of 1–2 week gaps occurring sporadically in the data set.

2.2. Identification of Key Events and Periods of Annual Fast Ice Cycle

Seasonal development of fast ice area in the southeastern Laptev Sea follows a characteristic pattern (Figure 2) with a rapid advance of fast ice in fall, small variability in winter and rapid decline in summer. We defined five key events describing this pattern (Figure 3): beginning of fast ice season (Key event 1), beginning and end of the rapid development (Key events 2 and 3), beginning of breakup (Key event 4), and end of fast ice season (Key event 5). These events were identified automatically using arbitrary thresholds for fast ice area and speed
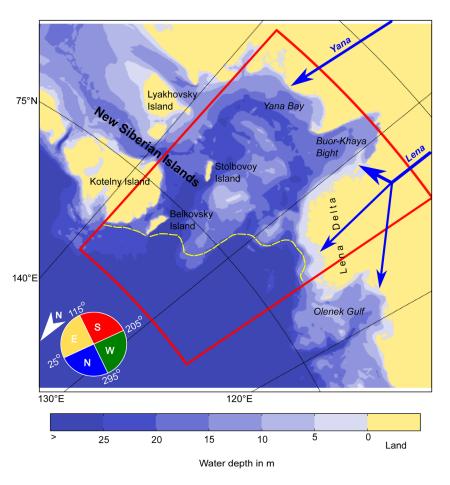
Figure 1. Region of interest and bathymetry. The red box indicates the area of the southeastern Laptev Sea for which the analysis was performed. The dash line shows the mean maximal fast ice extent between 1999 and 2013. The compass rose in the bottom left corner shows the four sectors (N, E, S, and W) which correspond to the analyzed wind directions (see section 2.4.4).

of areal growth presented in Table 1. The date of a specific key event is related to the date of chart issue. Because the maps are made from up to 1 week old information, the event dates may be biased up to 6 days. We assume that the error associated to this is normally distributed. The key events divide the fast ice season six periods: Period 1: Preformation, Period 2: Initial formation, Period 3: Rapid development (RDP), Period 4: Period of maximal extent, Period 5: Breakup (Figure 3).

2.3. Accuracy of AARI Charts

AARI does not provide an uncertainty estimate for the operational charts produced since 1998. However, the errors in ice edge location for the chart issued before 1998 vary from 2–10 [*Polyakov et al.*, 2003] to 50 km [*Mahoney et al.*, 2008]. In general, the quality of operational sea ice charts depends strongly on the resolution of the input data and the expertise of sea ice analysts. With the introduction of high-resolution satellite data in the mapping process after 1998, the quality of charts was significantly improved. In order to assess the quality of AARI charts for the period of our investigation, we compared them with fast ice maps derived from ENVISAT Synthetic Aperture Radar (SAR) imagery. The SAR images were acquired for the southeastern Laptev Sea between 2003 and 2012 and have a pixel resolution of 150×150 m. The fast ice edge was mapped manually based on visual discrimination between motionless fast ice and drifting pack ice from consecutive image pairs. The average time span between images in a pair is 3–7 days, which is consistent with the frequency of fast ice maps issued by AARI. Like the AARI charts SAR-based maps represent snapshots of fast ice extent on the date of the latest image in a pair. Overall, we obtained 73 maps of fast ice extent from the time series of SAR images. Most of the SAR scenes were acquired between January and April, when fast ice was at its maximal winter extent. Only a few scenes cover the RDP and no scenes were acquired during Breakup period.
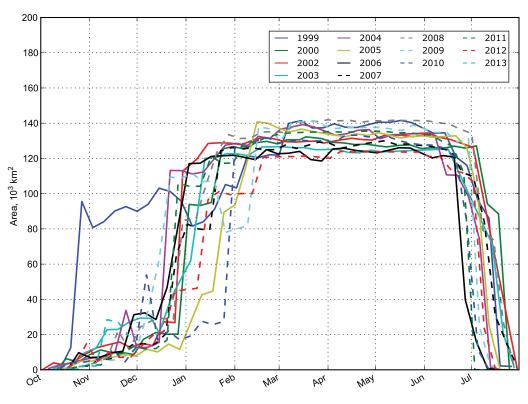
Figure 2. Annual cycle of fast ice area between 1999 and 2013.

Figure 4 shows a cross comparison of fast ice areal extent between the SAR-based data and the AARI charts. The difference between the data sets is smallest when fast ice extent is relatively small or close to the maximum. The highest deviations correspond to the RDP. By interpretation of SAR images, we encountered difficulties discriminating between pack ice and fast ice during this period, since the transition from drifting to motionless state is often subtle. Therefore, it is likely that the differences between the data sets during the
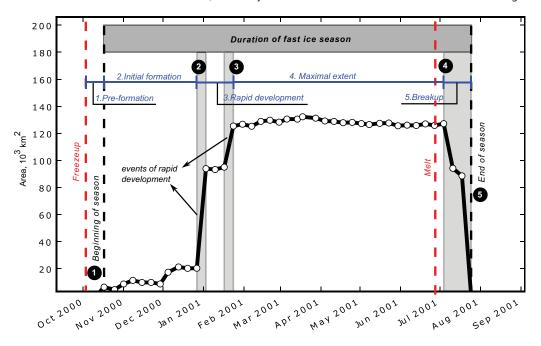

Figure 3. A typical annual fast ice cycle (2000–2001). The key events are numbered and the periods of annual fast ice cycle are labeled in blue.

Table 1. Key Events and Identification Criteria

Key Event	Identification Criteria
Beginning of season	Fast ice area reaches 5×10^3 km² ($\sim$4% of maximal area) correspond to narrow strip of fast ice along the coast
Beginning of RDP	Beginning of the first event when the speed of mean weekly areal development exceeds 14×10^3 km²
End of RDP	End of the last event when the speed of mean daily weekly development exceeds 14×10^3 km²
Beginning of breakup	Beginning of the first event when the speed of mean weekly areal decrease exceeds 10.5×10^3 km²
End of breakup/End of season	Fast ice area drops below 5×10^3 km² ($\sim$4% of maximal area)

RDP are attributed to subjective classification of sea ice types. Due to the high inaccuracies in fast ice classification, we neglected the single events of rapid development (Figure 3) and considered only the dates of the beginning and end of the period (Key events 2 and 3). Excluding the RDP, we estimated the mean deviation between the two data sets as $2.0 \times 10^3 \pm$ of 2.3×10^3 km².
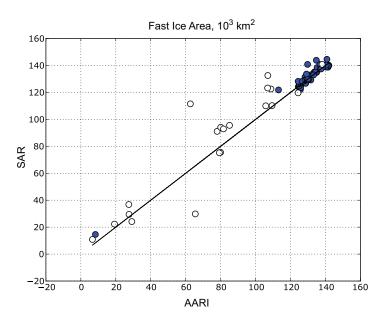
2.4. Ancillary Data
2.4.1. Bathymetry

We used the International Bathymetric Chart of the Arctic Ocean (IBCAO Version 3 [*Jakobsson et al.*, 2012]) in order to retrieve water depth at the location of the fast ice edge for every AARI chart. The IBCAO grid is in Polar Stereographic projection and has a resolution of 500×500 m. It was regridded to the 1.25 km EASE-Grid by nearest neighbor interpolation. Since the IBCAO depths for the Russian marginal seas are primarily derived from Russian nautical charts contours, the distribution of water depths in the region shows artificial modes at water depths multiple of 5. In order to remove the artificial modes, we used 5 m bin width to derive histograms of water depth occupied by fast ice edge.

2.4.2. Onset of Freezeup and Melt

To link the key events of the annual fast ice cycle to the onset of freezing and melting season, we used the Arctic-wide maps of freezeup and melt onset derived from SSM/I/SMMR brightness temperatures [*Markus et al.*, 2009]. The data are mapped to the 25 km polar stereographic grid and contain information on dates of early (the first occurrence of melting/freezing conditions) and permanent freezeup/melt. In this study, we define freezeup and melt onset as the mean dates of the first occurrence of freezing or melting conditions in the region.

2.4.3. Freezing and Thawing Degree Days

We examined cumulative freezing (FDDs) and thawing (TDDs) degree days in order to understand the influence of air temperatures on seasonal development and interannual variations in fast ice extent. Cumulative degree days were calculated from NCEP daily 2 m air temperature [*Kalnay et al.*, 1996]. First, mean daily air temperatures for the region of interest were extracted. Then, FDDs were calculated as a sum of negative temperatures since the onset of freezeup. TDDs were calculated as a sum of positive temperature since the onset of melt.

2.4.4. Wind Speed and Direction

In order to analyze the effect of different wind directions and speed on the evolution of fast ice area, we derived wind speeds for four directions (N, E, S, and W) shown in Figure 1. Taking into account that on average the ice drift deviates by 20° [*Leppäranta*, 2011] from the wind direction, the wind sectors

Figure 4. Cross comparison of fast ice area derived from AARI charts and SAR imagery between 2003 and 2012. The white circles correspond to area estimates made during the RDP, and the blue circles indicate estimates made outside this period.

were set in a way that N and E correspond to the wind advecting ice offshore from the mainland (N) and the Lena Delta (E), and S and W wind cause onshore ice drift. The wind analysis was performed for four periods of annual fast ice cycle: Preformation, Initial formation, Rapid development, and Breakup periods. First, 6-hourly wind speed and direction were derived from the reanalysis data (NCEP 10 m wind) [*Kalnay et al.*, 1996] for the region of interest. Then the scalar wind speed values were assigned to one of four sectors based on the direction. For each period, we derived sector's mean wind speed as a sum of wind speeds in a sector divided by a total number of measurements for a period. Therefore, the mean wind speed of a sector characterizes the intensity of the wind for the individual periods. In the following, we compare the duration of the four periods with the mean wind speed in four directions.

2.4.5. Lena River Runoff and Breakup

To identify the date of Lena River breakup, we use the discharge data from the Kusur gauging station (70.70°N/127.65°E) located around 200 km south of the Lena Delta. According to *Bareiss et al.* [1999], breakup of fast ice in the vicinity of the Lena Delta is associated with the breakup of the Lena River. The authors find the strongest connection between the annual maximal discharge at Kusur station and early sea ice melt signal. To be consistent with their study, we define the Lena River breakup as the date when spring discharge at the Kusur station reaches its maximal value.

3. Results

3.1. Variability of Fast Ice Extent

Figure 2 shows 14 annual cycles of fast ice development from October to July. It illustrates that the interannual variability of fast ice extent is very low in February–June and higher in October–January and July. In most years, the extent is within 12.8×10^3 km^2 of the 14 years mean for any given week of a month (for February–June) and within 37.5×10^3 km^2 (for October–January and June). Only two annual cycles (1999 and 2009) showed an exceptional behavior. In fall 1999, fast ice started to develop remarkably early, after which the development of fast ice area slowed down and the winter extent was reached relatively late in the season. The year 2009 is characterized by a distinct winter breakup event in January–February, which was not observed in any of the other 12 annual cycles.

The spatial variability of fast ice extent can be seen in Figure 5. The monthly maps were derived by stacking all available AARI charts for each calendar month. High occurrence regions (shown in red) indicate the patterns of fast ice extent common to each calendar month, while regions with lower fast ice occurrence provide information on interannual variability (e.g., the exensive blue region in October corresponds to the early advance in 1999). As Figure 5 illustrates, fast ice starts forming as a narrow band along the Lena Delta shore, and the Yana Bay in October–November. Next, fast ice fills the Buor-Khaya Bight. During December–January, fast ice expands in the north-west direction connecting the shore of Yana Bay with the New Siberian Islands. The fast ice edge east of the Lena Delta at this stage of development has a characteristic u-shaped configuration. The tendency of fast ice to advance into shallower waters first (see section 3.4) is demonstrated by the higher occurrence frequencies seen over the shoal north of Stolbovoy Island in December (Figure 5). In February–March, fast ice is still slowly advancing seaward, but the increase in area does not exceed 8%. The maximal extent is reached in March–April, and thereafter this, the fluctuations of the extent are very small and do not exceed 4.5%. The winter maximal extent does not vary significant from year to year (Table 2), as well as shape and location of fast ice edge at the maximal extent.

The first indication of fast ice breakup can be seen as a decrease in occurrence frequencies along the Lena Delta in Figure 5 in June. The summer breakup is more abrupt than the rapid development in fall. While in June, the fast ice area remains close to its maximum extent, there is no area in the Laptev Sea that remains covered by fast ice throughout the month of July for the entire observation period. Breakup of fast ice starts along the Lena Delta and progresses eastward. At the same time, the seaward fast ice edge retreats to the south. The fast ice cover in-between the New Siberian Islands breaks up last. This spatial pattern of fast ice disintegration is different to the advance of fast ice in fall. In fall, the fast ice advances in a southeast-to-northwest direction, while the summer fast ice edge retreats mainly from the west to the east. However, the u-shape pattern of low frequencies east of the Lena Delta is characteristic for both the advancement of fast ice in fall and its retreat in summer. This area becomes covered with fast ice last and gets free of fast ice first.
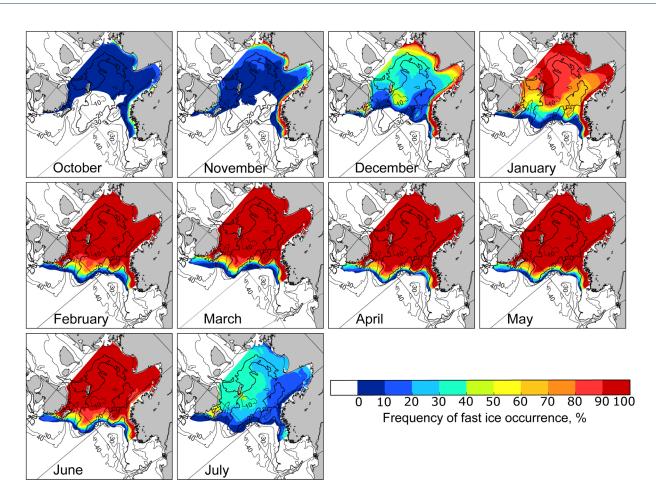
Figure 5. Monthly frequency of fast ice occurrence. The maps are derived by stacking all available fast ice maps for each calendar months. The color code represents at which fraction of the stacked maps fast ice was present. The isobaths are shown in black, thick contour corresponds to 20 m water depth.
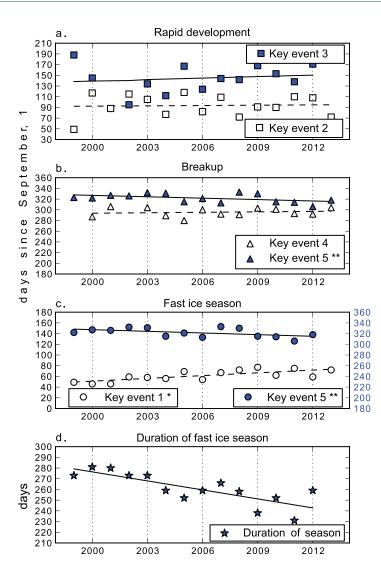
3.2. Timing of Key Events

We identified the timing of the key events described in section 2.2 in each of the annual fast ice cycles from 1999 to 2013. Due to a gap in the AARI data set in winter 2002, the identification of the Key events 3, 4, and 5 was not possible for this period.

The interannual variability and trends in the timing of the five key events and corresponding periods of annual fast ice cycle is shown in Figure 6. Minimal, maximal, and mean, as well as the standard deviation of the timing of key events are presented in Table 3. On average, the fast ice season starts on the first week of November, which is 25 ($\pm$8.4) days after the onset of freezeup. The season ends on the first week of June, 51 ($\pm$4.7) days after melt onset. The interannual variability in timing of the Key events 1 and 5 is remarkably low (Figure 6c). However, there are statistically significant tendencies toward later beginning and earlier end of fast ice season. These tendencies result in a decrease of the fast ice season by -2.9 d/yr (Figure 6d). The RDP starts between October and December. In three out of 14 seasons, the beginning of rapid development coincides with the onset of fast ice formation. For the other seasons, the time lag between these two key events (Key events 1 and 2) ranges between 2 and 11 weeks. The beginning and end of rapid development (Figure 6a) shows twice as high variability in timing compared to the other key event (Table 3). The duration of RDP varies from 1 to 13 weeks. The following period of Maximal extent lasts for 22 $\pm$ 4 weeks and its duration does not show any interannual changes. In contrast, the Breakup period tends to become shorter (Figure 6b).

Overall, the timing of the key events exhibits low interannual variability, except for the beginning and end of

Table 2. Variability of Maximal Areal Extent

	Area (10³ km²)				Date[a]		
Mean	SD	Min	Max	Mean	SD (days)	Min	Max
134.4	0.6 (4.5%)	123.9	141.9	13 Mar	34	6 Feb	3 Jun

[a]The first date after which areal increase does not exceed 4.5%.

Figure 6. Timing of key events and duration of corresponding periods of annual fast ice cycle. The events with star and two stars sign show a trend significant at 99% and 90% confidence level correspondingly.

rapid development. We also found trends in timing of the marginal events of the annual fast ice cycle. While timing of the beginning and end of the fast ice season is shifting, there are no statistically significant trends in the timing of the RDP, beginning of breakup, as well as duration of the Maximal extent period (Table 4).

3.3. Wind Speed and Direction

Figure 7 shows the time series of mean wind speeds over four periods of annual fast ice cycle (Periods 1, 2, 3, 5) for directions N, E, S, and W (for the definitions see section 2.4.4 and Figure 1) together with duration of the periods. The wind speeds are consistent between the periods and show low interannual variability. On average, the mean wind speed for any of the four sectors varies between 0 and 2 m s^{-1} rarely exceeding 3 m s^{-1}.

Comparing the duration of the four periods with the time series of wind speed, we found strong to moderate correlations for periods of Preformation and Initial formation and weak or no correlations for RDP and Breakup (Table 5).

Overall, correlations for the Preformation period are higher than for the other periods, indicating a stronger relationship with the wind forcing. Remarkably, the correlations for the offshore (N: $r = 0.48$, $p = 0.07$; E: $r = 0.73$, $p < 0.01$) and onshore (S: $r = -0.35$, $p = 0.21$; W: $r = -0.57$, $p = 0.03$) winds are comparable in magnitudes and have opposite signs. The duration of the Preformation period decreases with stronger onshore winds (S and W) and weaker offshore wind (N and E), and vice versa. This suggests the importance of mechanical fast ice growth due to advection of pack ice toward the shore.

Although the S winds show a strong correlation with the duration of Initial formation, there is no causal relationship between the variables. The positive relationship between the onshore sector and the duration of Initial formations is based on three extreme years, when the duration of Initial formation was minimal and characterized by absence of S winds. However, S wind is also absent in years with relatively long duration of Initial formation (e.g., 2001 and 2002). In addition, the wind speed and its variation are very low (below 1 m s^{-1}) throughout the time series.

Table 3. Variability of Dates of the Key Events

Key Event	Mean	SD (days)	Min	Max
1. Beginning of fast ice season	1 Nov	10	17 Oct	17 Nov
2. Beginning of RDP	2 Dec	20	20 Oct	28 Dec
3. End of RDP	23 Jan	24	5 Dec	7 Mar
4. Beginning of breakup	23 Jun	8	8 Jun	7 Jul
5. End of season	19 Jul	9	3 Jul	30 Jul

Table 4. Trends in Timing of Key Events and Periods of Annual Fast Ice Cycle

Key Event/Period	Trend (d/yr)	p	r^2	σ_{est}
1. Beginning of season	1.7	<0.01	0.56	0.4
2. Beginning of RDP	0.0	0.98	<0.01	1.3
3. End of RDP	0.4	0.07	0.02	1.6
4. Beginning of breakup	0.3	0.63	0.02	0.6
5. End of season	−1.0	0.06	0.26	0.5
Rapid development (RDP)	−0.3	0.92	<0.01	2.4
Maximal extent	−1.4	0.46	0.05	1.8
Breakup	−1.3	0.05	0.30	0.6
Fast ice season	−2.8	<0.01	0.63	0.6

3.4. Water Depth at Fast Ice Edge

In this section, we examine the variability of water depth occupied by the fast ice edge during the annual cycle. Figure 8 shows the distribution of depths at the location of the fast ice edge for each month. *Mahoney et al.* [2007a, 2014] suggest that the most frequently observed water depths correspond to the depth at which the fast ice edge is most stable. The water depths occupied by the fast ice edge show a unimodal distribution. In October, the mode is at 0–5 m depths. In the following 6 months, the dominant mode gradually shifts from 10–15 to 15–20 m to greater depths as fast ice expands. This range corresponds to the most frequent depths in the region and therefore the frequencies of fast ice occurrence are expected to be higher between 10 and 20 m. Fast ice edge reaches the deepest location in March–April with the most frequent occurrence between 20 and 25 m. The beginning of fast ice breakup in June is characterized by small changes in the water depths distribution. While a considerably large areal decrease takes place in July, the water depths distributions at the fast ice edge are very similar to those found during winter.
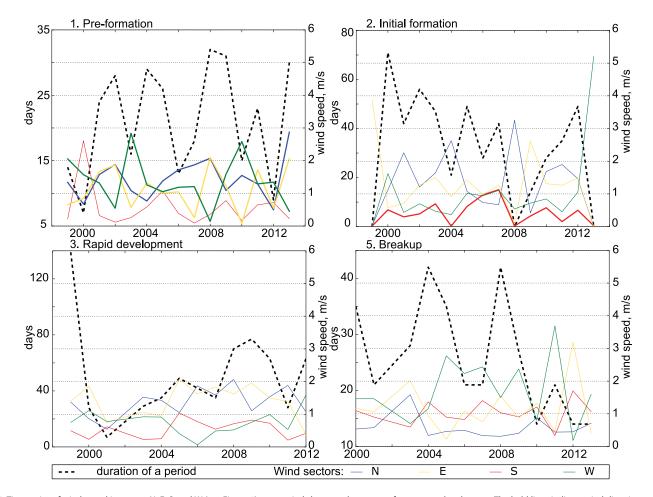

Figure 7. Time series of wind speed in sectors N, E, S, and W (see Figure 1) over periods between key events, freezeup, and melt onset. The bold lines indicate wind directions which have the highest correlation with the duration of the corresponding period (see Table 5).
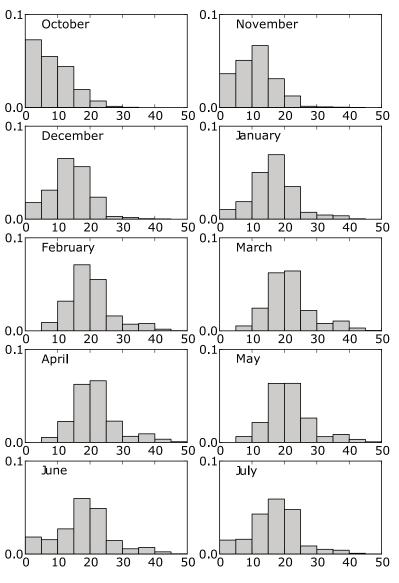
Figure 8. Monthly histograms of water depth at fast ice edge.

4. Discussion

In the following section, we link the seasonal and interannual variability of fast ice extent to the onset of freezeup and melt, air temperature (FDDs and TDDs), wind, bathymetry, and Lena River runoff. We follow the annual fast ice cycle and discuss each key event and period of fast ice development in the order they occur within a season.

4.1. Beginning of Fast Ice Season

To form a stable motionless fast ice band along the coast, newly formed sea ice needs to reach a certain thickness that allows it to withstand wind, tidal and wave action. According to observations from the Russian polar stations, formation of fast ice in the Laptev Sea starts when ice thickness reaches 5–10 cm, which takes place on average 10–15 days after freezeup [*Karklin et al.*, 2013]. Compared to these observations, our analysis shows a longer time lag between the freezeup onset and beginning of fast ice season (25 ± 8 days). The difference to the on-site observations is related to different definitions of the beginning of fast ice season. While observations refer to the first occurrence of fast ice at the coast, our definition corresponds to a more advanced stage of fast ice development (see section 1). Still, there is a strong correlation

Table 5. Correlation Between Wind Speed and Duration of Periods of Annual Fast Ice Cycle

Periods	N	p	E	p	S	p	W	p
1. Preformation	0.48	0.07	0.73	<0.01	−0.35	0.21	−0.57	0.03
2. Initial formation	0.08	0.79	−0.16	0.57	0.55	0.03	−0.19	0.49
3. Rapid development (RDP)	0.17	0.58	0.15	0.62	0.26	0.40	0.06	0.85
4. Breakup	−0.22	0.47	−0.15	0.59	−0.08	0.78	0.08	0.79

between the onset of freezeup and the beginning of fast ice season (Table 6). This suggests that the beginning of the fast ice season in the southeastern Laptev Sea is controlled to a large extent by thermodynamic processes.

Air temperatures and oceanic heat control sea ice growth rates and hence, the time needed to reach an ice thickness of 5–10 cm by thermodynamic growth, which is required to withstand external stresses. While year-round mooring observations from the deeper (>40 m) Laptev Sea shelf show surface warmed waters that may be trapped in the interior water column into fall and winter [*Janout et al.*, 2013], significant amounts of heat were not observed in the shallower waters within the fast ice zone. *Bauch et al.* [2009] reported on a temperature maximum in the intermediate water layer, which persister under fast ice until May in the immediate vicinity of the Lena River outflow. However, based on their temperature profile, the amount of heat stored would only melt the equivalent of 4 cm of ice and was capped by strong stratification. More recent under fast-ice profiles from the area taken in April 2012 were generally at near-freezing temperature, but showed that salinity stratification can persist throughout the winter (unpublished data, M. Janout (2015)). Late fall profiles from September 2013 and 2014 (unpublished data, M. Janout (2015)) from shallow nearshore areas either show a fresher warmer surface layer above a cold and saline lower layer, or a well-mixed water column by tides and winds. These data indicate that storage of a significant amount of heat in the shallow (<20 m) water is unlikely. The oceanographic conditions in the Laptev Sea fast ice area are such that warm ocean temperatures may delay the first formation of sea ice. However, considering that the fast ice season starts ∼3 weeks after the freezeup, oceanic heat does not have a considerable impact on the Laptev Seas fast ice processes.

In order to examine the influence of air temperature, we calculated FDDs between the onset of freezeup and the beginning of the fast ice season. As we consider the freezeup onset as a reference point for the calculations of FDDs, we assume that the water column is at a freezing temperature. Therefore, the FDDs reflect influence of the air temperature only. The high variability of FDDs (Table 7) indicates that the beginning of fast ice development is regulated by a dynamic component in addition to the thermodynamic processes.

It is difficult to distinguish between the influence of thermodynamic and dynamic factors on fast ice formation. While atmospheric and oceanic heat fluxes impact thermodynamic sea ice growth, the wind contributes to ice growth by rafting and ridging. The time lag between freezeup and the beginning of fast ice season can also be affected by local wind conditions. According to *Zubov* [1945], the onshore wind favors development of fast ice by pushing pack ice toward the coast, while offshore wind may slow down the advance of fast ice by dragging pack ice away from the fast ice edge. In the southeastern Laptev Sea, fast ice first starts to form along the eastern shore of the Lena Delta and in the Yana Bay (Figure 5). The corresponding offshore winds (N and E) delay the formation of fast ice in the region as reflected by a positive correlation between wind speed and the delay of fast ice season relative to freezeup (Table 5). The onshore winds (S and W) have the opposite effect on fast ice formation, confirming the hypothesis of *Zubov* [1945].

On interannual time scales, the beginning of the fast ice season exhibits the highest rate of change compared to other key events during the annual fast ice. The trend toward a later beginning of the fast ice season (1.7 d/yr) is consistent with a delayed freezeup (1.5 d/yr) in the region. Both trends are statistically significant at 99% confidence level. According to *Markus et al.* [2009], the Laptev Sea has the most significant delay in freezeup since 1996 compared to other Arctic

Table 6. Correlation Between Key Events, Freezeup, and Melt Onset and Lena River Breakup

Events	Freezeup	p	Lena River Breakup	p	Melt	p
Key event 1	0.62	0.01				
Key event 2	0.29	0.29				
Key event 3	0.55	0.05				
Key event 4			0.54	0.09	0.26	0.38
Key event 5			0.54	0.06	0.81	<0.01

Table 7. FDDs and TDDs Accumulated Prior the Key Events

Key Event	Mean	SD (%)	Min	Max
FDDS				
Key event 1	333	46	85	573
Key event 2	1119	43	203	1869
Key event 3	2578	27	1336	4095
TDDs				
Key event 4	31	46	8	55
Key event 5	83	18	57	112

marginal seas. Further changes in timing of freezeup onset are likely to be reflected in the timing of fast ice formation.

4.2. Rapid Development Period (RDP)

Because the AARI charts have the highest uncertainties during the RDP (see section 2.3), we did not investigate the advance of fast ice within this period, but we rather focused on the two key events—the beginning and end of rapid development (Key events 2 and 3). In terms of areal extent, both events are characterized by a low variability (Figure 2). Also, the configuration of fast ice at the end of the RDP is consistent throughout the 14 years of investigation (Figure 9). The high frequencies (70–100%) of fast ice occurrence coincide with the location of the shoals (Figure 1). Reoccurrence of the fast ice edge at the same locations indicates that this configuration of fast ice has a high stability. This stability can be obtained by grounding of fast ice at the shoals. During most years, the rapid development of fast ice stops once fast ice connects Kotelny Island with the shoals and the Lena Delta (Figure 9). Therefore, we suggest that the location of the fast ice edge at the end of the RDP is defined by the local bathymetry.

The beginning of the RDP does not appear to be linked with thermodynamic processes, since the timing of this key event is not correlated with the onset of freezeup (Table 6). In addition, the number of FDDs acquired prior to the beginning of rapid fast ice development exhibits high variability (Table 7). There are also no strong indications of a linkage between the wind forcing and timing of the event. Given the high variability in timing (Table 3), it is likely that the rapid development of fast ice is triggered by a combination of several processes which should be investigated using data sets of higher accuracies.

While it is not clear which mechanisms control the beginning of rapid development, there are indications that thermodynamics defines the duration of the RDP. First, there is a correlation between the freezeup onset and the end of rapid development. Second, the variability of FDDs at the end of the RDP is relatively low (Table 7), suggesting a linkage between the two. Also, we find that the duration of the period has a strong connection to FDDs (Figure 10). The longest duration of the RDP correspond to the year 1999, when minimal number of FDDs was acquired prior to the beginning of rapid development. Vice versa, when the number of FDDs increases, RDP spans over a shorter period. This relationship indicates that rapid fast ice development is closely linked to sea ice thickness growth. A relatively thin sea ice cover can stay motionless over the vast areas in calm conditions; however, it is prone to breakup under the action of strong wind. Although the quality of AARI charts within the RDP has to be treated cautiously, we assume that the decrease in fast ice area in fall 1999 (Figure 2) is related to a breakup of thin fast ice cover. Thick ice, on the other hand, is more resistant to the dynamic forcing and therefore it needs a shorter time to reach the stable configuration since its advance does not alternate with events of breakup. The low variability of FDDs at the end of the rapid development period indicates that at the time fast ice area approaches its winter extent, the thickness of fast ice is consistent from year to year. This confirms that mechanisms responsible for rapid fast ice development are dependent on sea ice thickness.

4.3. Period of Maximal Fast Ice Extent

The period of maximal fast ice extent corresponds to the time interval between the Key events 3 (end of rapid development) and 4 (beginning of breakup). Usually, by the end of the RDP, fast ice continues to expand at slow rate and reaches its absolute maximum in mid-March. On both interannual and seasonal time scales, the variations of maximal fast ice extent are very small. While local topography and bathymetry appear to define the stable configuration of the fast ice edge at the end of rapid development, it is unclear which factors control the further development of fast ice.

According to *Dmitrenko et al.* [1999], small variations in winter fast ice extent are defined by the intensity of Lena River runoff and location of the fresh water plume. The fresh riverine water overflows more saline water heated by solar radiation during summer. The resulting strong stratification preserves the heat in the intermediate water layer. *Dmitrenko et al.* [1999] suggest that this heat is released during fall and winter at the periphery of the river plume which affects the location of fast ice edge. However, a comparison of the
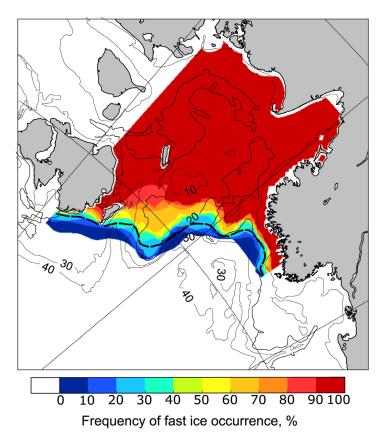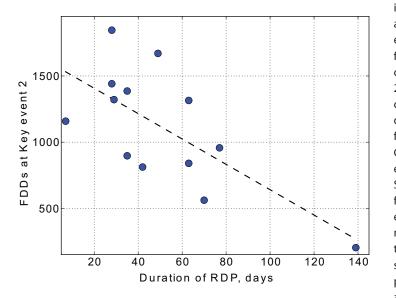
AARI winter fast ice extent with hydrographic patterns does not confirm the findings of *Dmitrenko et al.* [1999]. For example, according to hydrographic surveys in the southeastern Laptev Sea, the winters of 2008 and 2009 were characterized by substantially different surface salinity patterns [*Dmitrenko et al.*, 2010]. In 2008, Lena River outflow was shifted eastward by predominant westerly winds. In contrast, in 2009, river water accumulated near the Lena Delta due to easterly winds over the East Siberian Sea and northerly winds over the Laptev Sea. Although both hydrographic patterns differed from the long-term mean surface salinity distribution, we did not find significant variations between these two seasons in the winter location of the fast ice edge, its areal extent and transition through the annual key events.

Figure 9. Frequency of fast ice occurrence (%) at the end of RDP (Key event 3). The dash line shows the mean maximal fast ice extent between 1999 and 2013.

Bathymetry is another factor which is widely associated with the fast ice edge in winter, since the fast ice edge often reshapes isobaths of different depth. Along the Siberian coast the fast ice edge occupies depths of 20–25 m [*Zubov*, 1945]. These depths are characteristic for a typical location of fast ice edge in the southeastern Laptev Sea in March–April. In the Alaskan Arctic, there is a similar overall relationship between fast ice extent and bathymetry, which appears to depend on the presence of recurring grounded ice features distributed along the coast in water depths around 20 m [*Mahoney et al.*, 2014]. In contrast, Laptev Sea fast ice lacks deformation features along the fast ice edge [*Eicken et al.*, 2005]. Given that the maximal fast ice extent in the southeastern Laptev Sea does not differ significantly from the fast ice extent at the end of RDP, we suggest that the maximal winter extent is predetermined by the location of the shoals, where the ice is presumably grounded. Further advancement of fast ice to the greater water can result from a combination of several processes,

Figure 10. Scatterplot between the duration of RDP and FDDs acquired prior to the beginning of rapid development (Key event 2). The correlation coefficient between the variables is -0.70 ($p < 0.01$).
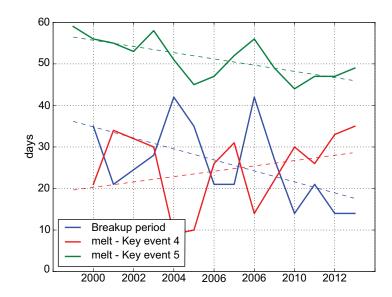
Figure 11. The duration of Breakup period and time lags between melt onset and Key events 4 and 5. The correlation coefficient between the duration of Breakup period (blue) and time intervals between melt onset and Key event 4 (red) and melt onset and Key event 5 (green) are -0.89 ($p < 0.01$) and 0.46 ($p = 0.12$), correspondingly.

i.e., mechanical attachment of pack ice during onshore drift events (or in absence of ice drift), as well as attachment of young ice formed at the fast ice edge during a polynya event. Since the changes in fast ice extent are rather small after the end of RDP, based on this study it is impossible to attribute them to individual physical processes.

Despite the reported warming and overall reduction of fast ice extent in the Arctic [*Yu et al.*, 2014], we did not find statistically significant trends in maximal fast ice extent. Investigating the variability of fast ice extent between 1979 and 2007, *Yu et al.* [2014] analyze the mean fast ice extent from January through March from operational charts. As fast ice is still advancing during January (Figure 5), the area of fast ice in this month does not reflect changes in maximal winter extent. We suggest that the reduction in fast ice area reported by *Yu et al.* [2014] is partly associated with a shift in timing of key events and shortening of Maximal extent period rather than the loss of the lateral extent.

4.4. Breakup Period and End of Fast Ice Season

Breakup of fast ice in the Laptev Sea is linked with Lena River breakup [*Bareiss et al.*, 1999; *Bauch et al.*, 2013]. The role of the spring river runoff is twofold: (1) overflowing fast ice, riverine water decreases the surface albedo and (2) it contributes to the direct input of heat. In their investigation *Bareiss et al.* [1999] concluded that the river input plays only a local role in breakup near the Lena Delta and the major part of fast ice breaks up and melts due to atmospheric forcing. The pattern of fast ice retreat in July (Figure 5) also suggests a strong impact of river discharge on the breakup processes. The lowest frequencies of fast ice occurrence correspond to the area of Lena River discharge. As the fast ice breaks up along the shore, it continues to retreat eastward. The area of open water formed along the Lena Delta facilitates lateral melt of fast ice. A similar mechanism takes place in the vicinity of the Yana River mouth. The fast ice edge there retreats from the shore northward. As a result, fast ice shrinks to the center of the southeastern Laptev Sea where it is stabilized by the New Siberian Islands. Hence, the distribution of the water depths at the fast ice edge remains similar to winter months (Figure 8).

The timing of fast ice breakup does not show any significant changes during the period of investigation. Confirming the results of *Bareiss et al.* [1999], we find a positive correlation between the Lena River breakup and the beginning of fast ice breakup (Table 6). The timing of Lena River breakup shows a small negative trend of -0.5 d/decade between 1935 and 2011, which is not observed on a shorter time scale. Moreover, the Lena River discharge in May increased by 63% since 1935 [*Yang et al.*, 2002]. Consequently, more heat is provided by the river runoff at the beginning of the breakup period. Taking into account a strong relationship between the river breakup and breakup of fast ice and the long-term changes in Lena River hydrography, it is likely that the timing of fast ice breakup is also shifting on a longer time scale.

In contrast to the beginning of breakup, the end of the fast ice season is strongly correlated to the onset of melt (Table 6) and it is tending to occur earlier in the season (Table 4). This tendency contributes to the shortening of the breakup period. However, the time lag between the onset of melt and beginning of fast ice breakup appears to have a stronger influence on the duration of the breakup period than the onset of melt itself (Figure 11). An increasing time lag between onset of melt and beginning of breakup allows for

higher TDDs to be accumulated prior the breakup. As a consequence ice becomes more permeable due to higher porosity and/or presence of cracks. Therefore, the river water is not spread as far as in case of cold and less permeable ice and its sensible heat is transferred in a smaller region. However, the influence of this process on fast ice breakup can act in both directions. On one hand, the localized transport of sensible heat will lead to an increased internal melting of fast ice. On the other hand, the effect of decrease albedo will affect only a small area of the fast ice cover.

5. Conclusions

By using AARI operational sea ice charts, we analyzed seasonal and interannual variability of fast ice extent in the southeastern Laptev Sea between 1999 and 2013. We identified five key events in each annual fast ice cycle and linked the occurrence of these events to freezeup and melt onset, air temperature (FDDs and TDDs), wind, bathymetry, and Lena River breakup. The analysis reveals that fast ice in the region is sensitive to thermodynamic processes throughout a season, while the wind has an influence only on the first stages of fast ice development.

The beginning of fast ice season is correlated to the onset of freezeup in the region and the delay between freezeup and formation of fast ice is affected by wind. Eastward and southward winds drag pack ice away from the shore of the Lena Delta and Yana Bay where fast ice forms first, delaying the beginning of fast ice season. Westerly and northerly winds favor earlier formation of fast ice.

While it is not clear what triggers the following rapid development of fast ice, the advance of fast ice is likely controlled by ice thickness growth, as certain ice strength is required to withstand dynamic forces. The persistence of the fast ice edge at the same location at the end of the RDP suggests that the bathymetry and local topography are important factors controlling lateral extent of fast ice.

The variations in winter fast ice extent are very small. Although the changes in maximal fast ice extent were previously attributed to the variability of FDDs and Lena River spring discharge, we did not find any connection to these factors.

Confirming the findings of *Bareiss et al.* [1999] we found a correlation between the Lena River breakup and beginning of fast ice breakup. The duration of breakup period has a strong relationship to the number of TDDs obtained between the onset of melt and Lena River breakup.

Analyzing the timing of the fast ice key events, we found a decrease in duration of fast ice season of 2.8 d/yr. The rate of changes in the duration of fast ice season during the last 14 years is stronger than the one reported for the period between 1979 and 2007 by *Yu et al.* [2014]. The changes in the duration of fast ice season are caused by both a later beginning and earlier end of fast ice season. In its turn, an earlier end of fast ice season is related to a shortening of the period required for fast ice breakup.

References

Are, F., and E. Reimnitz (2000), An overview of the Lena River Delta setting: Geology, tectonics, geomorphology, and hydrology, *J. Coastal Res.*, 16(4), 1083–1093.

Bareiss, J., and K. Gorgen (2005), Spatial and temporal variability of sea ice in the Laptev Sea: Analyses and review of satellite passive-microwave data and model results, 1979 to 2002, *Global Planet. Change*, 48(1–3), 28–54, doi:10.1016/j.gloplacha.2004.12.004.

Bareiss, J., H. Eicken, A. Helbig, and T. Martin (1999), Impact of river discharge and regional climatology on the decay of sea ice in the Laptev Sea during spring and early summer, *Arct. Antarct. Alp. Res.*, 31(3), 214–229, doi:10.2307/1552250.

Bauch, D., I. Dmitrenko, S. Kirillov, C. Wegner, J. Holemann, S. Pivovarov, L. Timokhov, and H. Kassens (2009), Eurasian Arctic shelf hydrography: Exchange and residence time of southern Laptev Sea waters, *Cont. Shelf Res.*, 29(15), 1815–1820, doi:10.1016/j.csr.2009.06.009.

Bauch, D., J. A. Holemann, A. Nikulina, C. Wegner, M. A. Janout, L. A. Timokhov, and H. Kassens (2013), Correlation of river water and local sea-ice melting on the Laptev Sea shelf (Siberian Arctic), *J. Geophys. Res. Oceans*, 118, 550–561, doi:10.1002/jgrc.20076.

Comiso, J. C., and D. K. Hall (2014), Climate trends in the Arctic as observed from space, *WIREs Clim. Change*, 5(3), 389–409, doi:10.1002/Wcc.277.

Divine, D., R. Korsnes, and A. Makshtas (2003), Variability and climate sensitivity of fast ice extent in the north-eastern Kara sea, *Polar Res.*, 22(1), 27–34.

Divine, D. V., R. Korsnes, and A. P. Makshtas (2004), Temporal and spatial variation of shore-fast ice in the Kara Sea, *Cont. Shelf Res.*, 24(15), 1717–1736, doi:10.1016/j.csr.2004.05.010.

Divine, D. V., R. Korsnes, A. P. Makshtas, F. Godtliebsen, and H. Svendsen (2005), Atmospheric-driven state transfer of shore-fast ice in the northeastern Kara sea, *J. Geophys. Res.*, 110, C09013, doi:10.1029/2004JC002706.

Dmitrenko, I., V. Gribanov, H. Kassens, and H. Eichen (1999), Impact of river discharge on the sea land fast ice extension in the Russian Arctic shelf area, paper presented at the 15th International Conference on Port and Ocean Engineering under Arctic Conditions, POAC'99, Espoo, Finland.

Dmitrenko, I. A., S. A. Kirillov, T. Krumpen, M. Makhotin, E. P. Abrahamsen, S. Willmes, E. Bloshkina, J. A. Holemann, H. Kassens, and C. Wegner (2010), Wind-driven diversion of summer river runoff preconditions the Laptev Sea coastal polynya hydrography: Evidence from summer-to-winter hydrographic records of 2007–2009, *Cont. Shelf Res.*, *30*(15), 1656–1664, doi:10.1016/j.csr.2010.06.012.

Eicken, H., I. Dmitrenko, K. Tyshko, A. Darovskikh, W. Dierking, U. Blahak, J. Groves, and H. Kassens (2005), Zonation of the Laptev Sea landfast ice cover and its importance in a frozen estuary, *Global Planet. Change*, *48*(1–3), 55–83, doi:10.1016/j.gloplacha.2004.12.005.

Herman, A., and O. Glowacki (2012), Variability of sea ice deformation rates in the Arctic and their relationship with basin-scale wind forcing, *Cryosphere*, *6*(6), 1553–1559, doi:10.5194/tc-6-1553-2012.

Hughes, N. E., J. P. Wilkinson, and P. Wadhams (2011), Multi-satellite sensor analysis of fast-ice development in the Norske Oer ice barrier, northeast Greenland, *Ann. Glaciol.*, *52*(57), 151–160.

Jakobsson, M., et al. (2012), The international bathymetric chart of the Arctic Ocean (IBCAO) version 3.0, *Geophys. Res. Lett.*, *39*, L12609, doi: 10.1029/2012GL052219.

Janout, M. A., J. Holemann, and T. Krumpen (2013), Cross-shelf transport of warm and saline water in response to sea ice drift on the Laptev Sea shelf, *J. Geophys. Res. Oceans*, *118*, 563–576, doi:10.1029/2011JC007731.

Johannessen, O. M., Y. I. Alexandrov, Y. Frolov, S. Sandven, M. Miles, L. P. Bobylev, L. H. Pettersson, and E. U. Smirnov, V. G. and Mironov (2005), *Remote Sensing of Sea Ice in the Northern Sea Route: Studies and Applications, Geophys. Sci.*, Springer, Chichester, U. K.

Kalnay, E., et al. (1996), The NCEP/NCAR 40-year reanalysis project, *Bull. Am. Meteor. Soc.*, *77*(3), 437–471, doi:10.1175/1520-0477(1996)077<0437:Tnyrp>2.0.Co;2.

Karklin, V. P., I. D. Karelin, A. V. Yulin, and E. A. Usol'tseva (2013), Osobennosti formirovaniya pripaya v more Laptevyh, *Probl. Arktiki i Antarktiki*, *3*(97), 5–14.

Kwok, R., G. F. Cunningham, M. Wensnahan, I. Rigor, H. J. Zwally, and D. Yi (2009), Thinning and volume loss of the Arctic Ocean sea ice cover: 2003–2008, *J. Geophys. Res.*, *114*, C07005, doi:10.1029/2009JC005312.

Laxon, S. W., et al. (2013), Cryosat-2 estimates of Arctic sea ice thickness and volume, *Geophys. Res. Lett.*, *40*, 732–737, doi:10.1002/grl.50193.

Leppäranta, M. (2011), *The Drift of Sea Ice*, Springer, Berlin, doi:10.1007/978-3-642-04683-4.

Mahoney, A., H. Eicken, A. G. Gaylord, and L. Shapiro (2007a), Alaska landfast sea ice: Links with bathymetry and atmospheric circulation, *J. Geophys. Res.*, *112*, C02001, doi:10.1029/2006JC003559.

Mahoney, A., H. Eicken, and L. Shapiro (2007b), How fast is landfast sea ice? A study of the attachment and detachment of nearshore ice at Barrow, Alaska, *Cold Reg. Sci. Technol.*, *47*(3), 233–255, doi:10.1016/j.coldregions.2006.09.005.

Mahoney, A. R., R. G. Barry, V. Smolyanitsky, and F. Fetterer (2008), Observed sea ice extent in the Russian Arctic, 1933–2006, *J. Geophys. Res.*, *113*, C11005, doi:10.1029/2008JC004830.

Mahoney, A. R., H. Eicken, A. G. Gaylord, and R. Gens (2014), Landfast sea ice extent in the Chukchi and Beaufort seas: The annual cycle and decadal variability, *Cold Reg. Sci. Technol.*, *103*, 41–56, doi:10.1016/j.coldregions.2014.03.003.

Maqueda, M. A. M., A. J. Willmott, and N. R. T. Biggs (2004), Polynya dynamics: A review of observations and modeling, *Rev. Geophys.*, *42*, RG1004, doi:10.1029/2002RG000116.

Markus, T., J. C. Stroeve, and J. Miller (2009), Recent changes in Arctic sea ice melt onset, freezeup, and melt season length, *J. Geophys. Res.*, *114*, C12024, doi:10.1029/2009JC005436.

Meier, W. N., et al. (2014), Arctic sea ice in transformation: A review of recent observed changes and impacts on biology and human activity, *Rev. Geophys.*, *52*, 185–217, doi:10.1002/2013RG000431.

Polyakov, I. V., G. V. Alekseev, R. V. Bekryaev, U. S. Bhatt, R. Colony, M. A. Johnson, V. P. Karklin, D. Walsh, and A. V. Yulin (2003), Long-term ice variability in Arctic marginal seas, *J. Clim.*, *16*(12), 2078–2085, doi:10.1175/1520-0442(2003)016<2078:Liviam>2.0.CO;2.

Polyakov, I. V., J. E. Walsh, and R. Kwok (2012), Recent changes of Arctic multiyear sea ice coverage and the likely causes, *Bull. Am. Meteorol. Soc.*, *93*(2), 145–151, doi:10.1175/Bams-D-11-00070.1.

Proshutinsky, A., I. Ashik, S. Hakkinen, E. Hunke, R. Krishfield, M. Maltrud, W. Maslowski, and J. Zhang (2007), Sea level variability in the Arctic Ocean from AOMIP models, *J. Geophys. Res.*, *112*, C04S08, doi:10.1029/2006JC003916.

Rachold, V., M. N. Grigoriev, F. E. Are, S. Solomon, E. Reimnitz, H. Kassens, and M. Antonow (2000), Coastal erosion vs riverine sediment discharge in the Arctic Shelf seas, *Int. J. Earth Sci.*, *89*(3), 450–460, doi:10.1007/s005310000113.

Rothrock, D. A., Y. Yu, and G. A. Maykut (1999), Thinning of the arctic sea-ice cover, *Geophys. Res. Lett.*, *26*(23), 3469–3472, doi:10.1029/1999GL010863.[10.1029/1999GL010863]

Spreen, G., R. Kwok, and D. Menemenlis (2011), Trends in Arctic sea ice drift and role of wind forcing: 1992–2009, *Geophys. Res. Lett.*, *38*, L02502, doi:10.1029/2011GL048970.

World Meteorological Organisation (2013), ''Global Digital Sea Ice Data Bank Project''—WDCB Sea Ice. Arctic and Antarctic Research Institute 7-days period generalized ice charts for the Russian Arctic and seasonal ice cover seas and the Greenland Sea for 1998–2013, St. Petersburg, Russia. [Available at http://wdc.aari.ru/datasets/d0004/.]

Yang, D. Q., D. L. Kane, L. D. Hinzman, X. B. Zhang, T. J. Zhang, and H. C. Ye (2002), Siberian Lena River hydrologic regime and recent change, *J. Geophys. Res.*, *107*(D23), 4694, doi:10.1029/2002JD002542.

Yu, Y. L., H. Stern, C. Fowler, F. Fetterer, and J. Maslanik (2014), Interannual variability of Arctic landfast ice between 1976 and 2007, *J. Clim.*, *27*(1), 227–243, doi:10.1175/JCLI-D-13-00178.1.

Zubov, N. N. (1945), *Arctic Sea Ice* [in Russian], Izd. Glavsevmorputi, Moscow.